



Synthesis, characterization and catalytic activity of new mesoporous Sr-based oxalate-phosphate-amine MOF

Awad I. Ahmed, Salem Elsayed Samra, Shaimaa Labeeb Ali

Chemistry Department, Faculty of Science, Mansoura University, Mansoura, Egypt

Received: 23/1/2020
Accepted: 17/2/2020

Abstract: Sr-based oxalate-phosphate-amine MOF was typically prepared under mild hydrothermal synthesis using anhydrous strontium nitrate $\text{Sr}(\text{NO}_3)_2$. Water as a green solvent, oxalic acid as the aliphatic linker, urea as the directing agent and orthophosphoric acid were used. The produced Sr-OPA-MOF has been typified by TEM, XRD, and FT-IR techniques. The synthesized MOF was found to exhibit outstanding catalytic activity on the formation of xanthene (14-phenyl-14H-dibenzo [a,j] xanthene).

keywords: Strontium-OPA-MOF, Hydrothermal synthesis, Xanthene reaction

1. Introduction

A new field, metal organic frameworks (MOFs), have come into view as auspicious crystalline materials in several areas for their flexible properties, typically built through the assembling of organic linkers and metal centers^[1]. Oxalate-phosphate-amine MOF (OPA-MOF) was first announced by Manuela Anstoetz in 2015^[2]. He has presented another green MOF in which the corner-sharing PO_4^- and FeO_6^- units can be associated through the oxalic acid ligand through two ways shaping a full-scale elastic system which conveys ammonium from disintegrated urea as visitors^[3]. The oxalate structure is a wellspring of vitality for oxalotrophic microorganisms and carbon by adequate solvency within soil arrangement, which empowers the carbonate biomineralization using the pathway of oxalate-carbon causing an expansion in the pH soil^[4]. OPA-MOF is synthesized according to the topology saying that the attached organic ligands, if possible, have multiple electron donors, like nitrogen and oxygen, during the conjunction with the structure directing agent to control the framework formation^[5]. For example, a widely investigated aliphatic ligand oxalic acid has unpredictable tasks in the framework acting as a bi- or multi-dentate ligand. In the field of plant soil systems, oxalate can also play the important roles identical to a chelator for the release of soil bound phosphorus; a design strongly used by plants to

recover P bioavailability^[6]. Inevitably, oxalotrophic bacteria exist in nearly any soil and use oxalate as a carbon source for their own metabolism, generating carbonates as a result through the oxalate-carbonate-pathway^[7]. Otherwise, Urea as a SDA can supply the main plant nutrient^[8]; N. It would surely have to be a di-amine as an environmentally benign, on account of toxicity that concerns from ethylenediamine, or similar in soil profiles. The urea procedure or uniform precipitation method is applied for the hydrothermal assembly of inorganic hydrous metal-oxide minerals. Through this method, the distribution of ammonium ions is homogeneous in the solution, affecting the solution H^+ gradient, which control the modification of product crystallinity^[9]. This theory assures Warner and Shaw's feedback about the urea decomposition in aqueous solutions. Researchers in MOF synthesis did not think about urea for controlling or medical applications, as small pores may form as objected to the considerably used bigger di-amines and organic linkers^[10]. A strategy to build a metal organic structure from the SDA (urea) with a Sr-phosphate backbone, and a moiety of an oxalate construction which basically be broken down microbially, attracted us a lot. Manuela Anstoetz has concentrated on OPA-MOF as manure yet in this research, we worry about the catalytic activity of Sr-OPA-MOF.

The medicate development industry has showed an inspiring effort toward xanthenes, first and foremost 14-phenyl-14H-dibenzo [a,j] xanthene. Xanthenes are formed through the condensation of β -naphthol with aromatic aldehydes in the existence of acid catalysts such as heteropoly acid supported boric acid^[11], MCM-41^[12], succinimide-N-sulfonic acid^[13] and silica attached N-propyl sulfamic acid^[14]. This is explained on the basis of a huge area of biological and pharmacological features like antiviral^[15], anti-inflammatory^[16], antifungal activities and antibacterial^[17], usage in photodynamic therapy^[18], dyes^[19], visualization of biomolecules through pH-sensitive fluorescent materials^[20] and laser technologies^[21] becoming to their attracting spectroscopic merits.

2. Experimental

2.1 Materials

All organic and inorganic chemicals utilized for the elaboration of catalysts such as strontium nitrate ($\text{Sr}(\text{NO}_3)_2$), orthophosphoric acid (H_3PO_4), oxalic acid ($\text{C}_2\text{H}_2\text{O}_4$) and urea ($\text{CH}_4\text{N}_2\text{O}$) were of analytical degree.

2.2 Preparation of Sr-OPA-MOF

The nanocatalyst was prepared under mild hydrothermal synthesis from a homogenous solution of strontium nitrate, orthophosphoric acid, oxalic acid, urea and water with molar ratios of (0.94:5.6:1:3:100), respectively. The mixture was exposed to ultrasonic for 10 mins, then was stirred at room temperature for 1 hour, put into a Teflon tube, and set into a pre-heated oven for 72 hours at 100°C. Then, the Teflon tube was taken away from the oven, cooled, washed several times with water and dried at 80°C^[22].

2.3 Techniques

2.3.1 X-ray diffraction analysis (XRD)

XRD patterns of the nanocatalyst was recorded using PW 150 (Philips), Cu $K\alpha$ radiation source and Ni channel at a low and high point. The instrument was worked at 40 kV and 45mA^[23]. The checking was made for 2θ point from 1 to 70 degrees, with a stage size of 0.02 and a stage time of 2 seconds. This apex is requested to a hexagonal unit cell and used identified with Bragg's law in figuring d100 isolating for the hexagonal pore mastermind

similarly as the unit cell parameter (a_o)^[24]. Bragg's law and its association with the unit cell parameter are fused into conditions (2-1) and (2-2). Where the ordinary crystallite size of particles was constrained by XRD line augmenting strategy using Debye-scherrer condition (2-3)

$$n\lambda = 2d_{100}\sin(\theta) \quad (2-1)$$

$$a_o = \frac{2d_{100}}{\sqrt{3}} \quad (2-2)$$

$$D = \frac{0.9\lambda}{\beta \cos \theta} \quad (2-3)$$

Where λ is radiation wavelength (Å), D is crystallite size, θ = angle of reflection and β is (radians) the line breadth^[25].

2.3.2 Transmission electron microscopy (TEM)

TEM tests were set up by dunking in a water suspension of smooth sample powders onto a copper grid covered with porous carbon foil and dried at a surrounding temperature. Transmission electron microscopy images and particle size were obtained utilizing JEOL-jem-2100 transmission electron microscope working at 120 KV^[26].

2.3.3 Fourier transform-infrared spectra (FT-IR)

Fourier transform infrared spectra of the meso-spongy frameworks were performed by utilizing the in situ FT-IR spectroscopic procedure on Nicolet magna-IR 550 spectrometer in the mid-IR region 400-4000 cm^{-1} through a 4 cm^{-1} resolution and 128 outputs. The sample was ground with KBr and squeezed into a dainty wafer which was set inside the IR cell and afterwards the range was recorded^[27].

2.4 Catalytic activity of Sr-OPA-MOF on 14-phenyl -14H-dibenzo [a,j] Xanthene synthesis

A reaction of β -naphthol (2 mmol) and benzaldehyde (1 mmol) with 0.10 g of the catalyst (activated at 120 °C for 2 h), was considered to obtain xanthene^[28]. The reaction was done with stirring for suitable time at 125 °C in a 50 mL flat bottomed flask. To check the completion of the reaction, the reaction was tested by TLC technique. After that, the product was dissolved in chloroform and the catalyst was separated through filtration and washed

with chloroform to reuse again. Aqueous ethanol (15%) was used for three times to recrystallize the yield. The yield% was calculated as follows^[29]:

$$\text{Yield (wt.\%)} = \left(\frac{\text{Obtained weight of product}}{\text{Theoretical weight of product}} \right) \times 100 \quad (2-4)$$

3. Results and discussion

3.1 X-ray diffraction analysis

In Fig.1, the low x-ray pattern of MOF shows typically two reflections between $2\theta = 0$ to 10° . The position of the peaks are $2\theta = 0.68^\circ$ ($d = 130.65 \text{ \AA}$), 2.39° ($d = 36.97 \text{ \AA}$). The low peaks data confirm the formation of mesoporous MOF sheets with superior crystallinity, porosity and intensity^[30]. From the high XRD data in Figure 2 between $2\theta = 10$ to 70° , a strong intense peak at around $2\theta = 14.49^\circ$ ($d = 6.11 \text{ \AA}$) is observed as evidence of Sr-MOF with oxalic acid as a linker existence^[22]. The peaks near 25° are indicative of amorphous carbon^[31, 32]. The MOF sheets have a characteristic peak at 2θ of $\sim 24^\circ$ which in turn resembles that of GO sheets^[33]. XRD analysis shows two distinct peaks at 18° and 30° imputed to phosphorous doping^[34]. Generally, the characteristic diffraction peaks of Sr-MOF have lower 2θ values indicating an increase in the lattice constants and the surface area. The results of crystallite size of the nanocatalyst concurred well with the consequence of crystallinity (%), the total area of all peaks and FWHM [$^\circ 2\theta$.] in the Table 1.

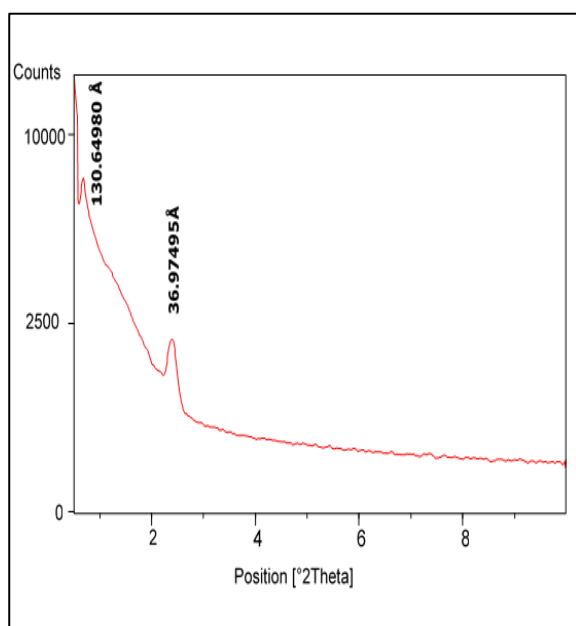


Fig.1. The low angle X-ray diffraction of

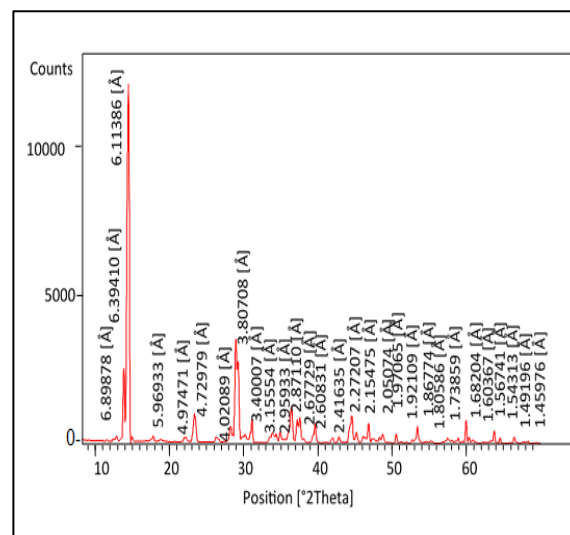


Fig.2. The high angle X-ray diffraction of Sr-OPA-MOF Sr-OPA-MOF.

Table.1. XRD parameters of Sr-OPA-MOF

The samples	Crystallite size D (nm)	%Crystallinity	Total area of allpeaks	FWHM [$^\circ 2\theta$.]
Sr-OPA-MOF	16.2	98.9	11496.27	0.4925

3.2 Transmission electron microscopy (TEM)

framework nanosheets which exhibit a high porosity (mesoporous MOF). The morphology of Sr-MOF may be displayed as a graphene like MOF as it is a Sr-MOF within C, N and P inside its pores^[33].

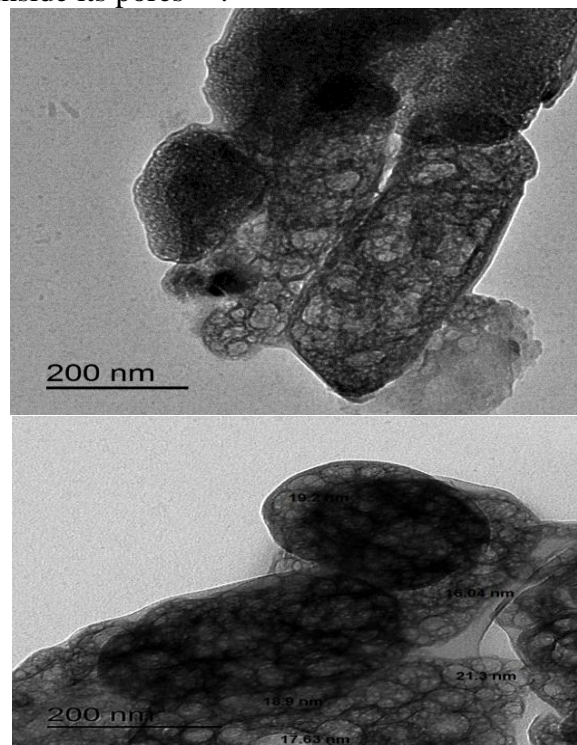


Fig.3. Transmission electron microscopy images of Sr-OPA-MOF.

3.3 Fourier transform-infrared spectra (FT-IR)

The FT-IR spectra of the MOF in Fig.4, exhibited the distinct stretching vibration of carboxylate anions at 1618 cm^{-1} , proving the nature of reaction of $-\text{COOH}$ groups in the oxalic acid with metal ions^[35]. The presence of water and $-\text{OH}$ groups in the structure of the material is proved through the outcrop of a broadband at 3497 cm^{-1} ^[36]. The band at 1316 cm^{-1} is associated with $\text{O}-\text{C}$ stretching^[37]. The region at 919 cm^{-1} can be referred to $\text{P}-\text{O}(\text{H})$ band^[38]. The sharp absorption bands at 956 cm^{-1} and 885 cm^{-1} can be accredited to out of plane bending vibration of $\text{Sr}-\text{O}$ ^[39]. The band at 2227 cm^{-1} is characteristic for $-\text{N}=\text{C}=\text{O}$, $-\text{N}=\text{C}=\text{N}$, and $\text{C}=\text{C}=\text{O}$ groups^[40, 41].

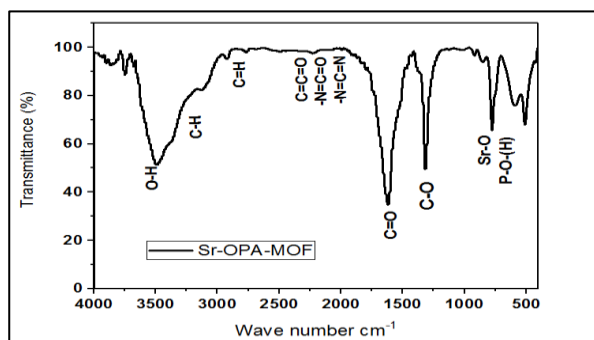


Fig.4. Fourier transform-infrared spectra of Sr-OPA-MOF

3.4 Catalytic activity of Sr-OPA-MOF on the synthesis of 14- phenyl -14H-dibenzo [a,j] xanthene

3.4.1 Effect of molar ratio of benzaldehyde : β -naphthol

The reaction was carried out over Sr-OPA-MOF, using different molar ratios of benzaldehyde and β -naphthol from 1:1, 1:1.5, and 1:2 to 1:3 at 125°C under solvent-free conditions. Fig.5 shows that 1:2 is the most suitable molar ratio of reactants. Further

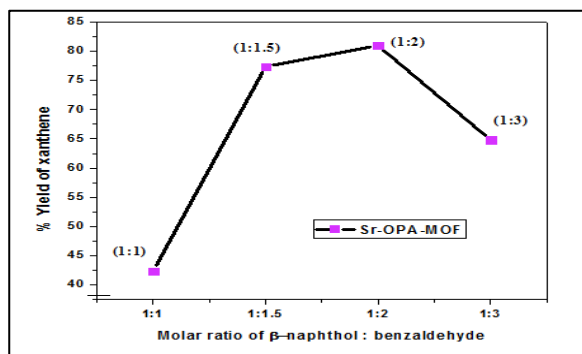


Fig.5. Effect of molar ratio of the reactants on the catalytic activity of Sr-OPA-MOF

3.4.2 The effect of different dosages of Sr-OPA-MOF

Different weights (0.02, 0.03, 0.05, 0.07, 0.1 and 0.2 g) of MOF were examined on xanthene synthesis as in Fig.6. The yield of reaction is increased from 33% to 81% with increasing the dosage of MOF from 0.02g to 0.05g. No worthy distinction was noticed during the amount of MOF was enhanced from 0.07g to 0.2g. The number of active sites on MOF rise with increasing the weight of MOF, which in turn, increases the synthesis average of xanthene, and that would raise the conversion rate.

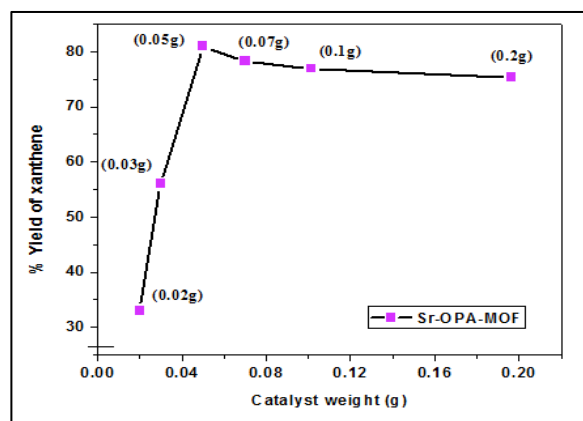


Fig.6. The effect of Sr-OPA-MOF dosages on of its activity.

3.4.3 Effect of different reaction times

The reaction was followed at different times from 30 to 180 mins. It was observed from the Fig.7 that the yield% increases progressively with increasing the time till reach maximum at 2 hrs (120 min), then become constant by increasing the time over 2 hrs. This indicates that the 2 hrs is the optimum time for the reaction to be completed.

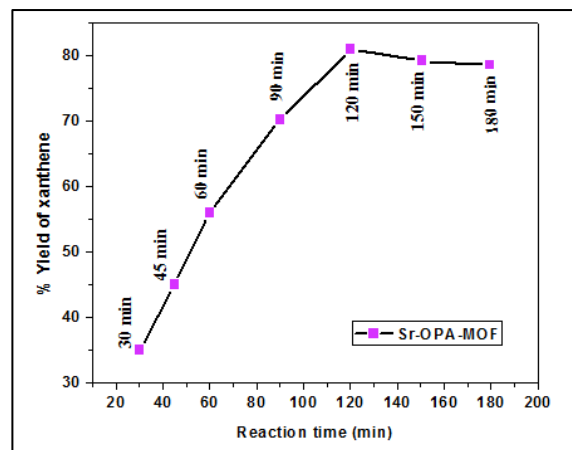


Fig.7. Effect of reaction times on the activity of Sr-OPA-MOF

3.4.4 Catalyst reusability

We examined the recycling of the Sr-OPA-MOF nanocatalyst three times in xanthene synthesis applying the same reaction conditions. Fig.8 illustrates that the MOF showed reusability after four runs. Decrease in the activity of Sr-OPA-MOF could be attributed to the loss in MOF weight.

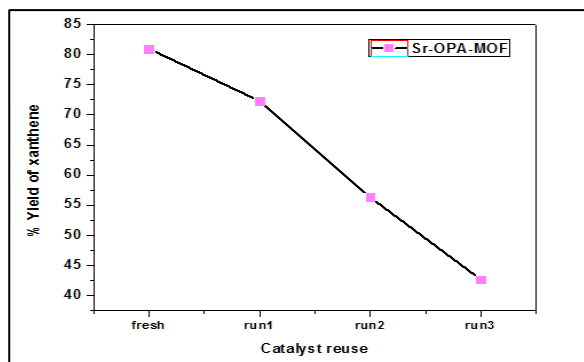


Fig.8. Catalyst reusability of Sr-OPA-MOF.

3.5 Conclusion

An eco-friendly oxalate-phosphate-amine-MOF with strontium (II) was synthesized under conditions of depressed urea ratio, low temperature, excess reaction time, elevated water ratio and was of high virtue with convenient P and N contents. The bi-dentate linker (oxalate bridges) between Sr-centers arranges the nanosheets, and then as pillars linking the nanosheets into a framework. A structural characterization of Sr-OPA-MOF by FT-IR, XRD and TEM demonstrated the formation of a mesoporous nanosheets of Sr-OPA-MOF that exhibited ultrahigh porosity and crystallinity. Using a facile protocol for the assembly of 14- phenyl -14H-dibenzo [a,j] xanthene from β -naphthol and benzaldehyde, has hopeful purposes such as high yield, generality, efficiency, cleaner reaction profile and recyclability which make it a salutary and charming process for the synthesis of xanthenes as biologically thought-provoking compounds. The % yield of xanthene reached a maximum value of 81% by (0.05g) of Sr-OPA-MOF after 2 hrs at 125°C.

4. References

- 1 Y., et al., (2017). A Sr²⁺-metal-organic framework with high chemical stability: synthesis, crystal structure and photoluminescence property. *Philosophical Transactions of the Royal Society A: Mathematical, Physical and Engineering Sciences*, **375**(2084): p. 20160026.
2. Anstoetz, M., (2016). Synthesis optimisation, characterisation and evaluation of an iron-based oxalate-phosphate-amine MOF (OPA-MOF) for innovative application in agriculture.
3. Anstoetz, M., et al., (2015). Novel applications for oxalate-phosphate-amine metal-organic-frameworks (OPA-MOFs): Can an iron-based OPA-MOF be used as slow-release fertilizer? *PloS one*, **10**(12): p. e0144169.
4. Anstoetz, M., et al., (2016). Characterization of an oxalate-phosphate-amine metal-organic framework (OPA-MOF) exhibiting properties suited for innovative applications in agriculture. *Journal of materials science*, **51**(20): p. 9239-9252.
5. Freeman, G., (2006) Access to Health Care Among Hispanic Or Latino Women, United States, 2000-2002. US Department of Health and Human Services, Centers for Disease Control and .
6. Yee, L.H., Manuela Anstoetz, Malcolm W. Clark &. (2017) *J Inorg Organomet Polym.*, **27**: p. 996-1013.
7. Martin, G., et al., (2012). Fungi, bacteria and soil pH: the oxalate-carbonate pathway as a model for metabolic interaction. *Environmental microbiology*, **14**(11): p. 2960-2970.
8. Lii, K.-H., et al., (1998). Syntheses and structures of organically templated iron phosphates. *Chemistry of materials*, **10**(10): p. 2599-2609.
9. Rajic, N., (2002). Principal component thermography for flaw contrast enhancement and flaw depth characterisation in composite structures. *Composite structures*, **58**(4): p. 521-528.
10. Aríñez-Soriano, J., et al., (2016) Single-crystal and humidity-controlled powder diffraction study of the breathing effect in a metal-organic framework upon water adsorption/desorption. *Chemical Communications*). **52**(45): p. 7229-7232.
11. Jaberi, Z.K., M.M.R. Shams, and B. Pooladian, *Expedition* (2013)., four-component synthesis of 1, 4-dihydropyrano [2, 3-c] pyrazole

- derivatives catalyzed by trichloroacetic acid or ceric sulfate. *Acta Chimica Slovenica*, **60(1)**: p. 105-108.
12. Mondal, J., et al., (2012). Functionalized mesoporous materials as efficient organocatalysts for the syntheses of xanthenes. *Journal of Molecular Catalysis A: Chemical*, **363**: p. 254-264.
 13. Shirini, F. and N.G. Khaligh, (2012). Succinimide-N-sulfonic acid: An efficient catalyst for the synthesis of xanthene derivatives under solvent-free conditions. *Dyes and Pigments*, **95(3)**: p. 789-794.
 14. Rashedian, F., D. Saberi, and K. Niknam, (2010). Silica-Bonded N-Propyl Sulfamic Acid: A Recyclable Catalyst for the Synthesis of 1, 8-Dioxo-decahydroacridines, 1, 8-Dioxo-octahydroxanthenes and Quinoxalines. *Journal of the Chinese Chemical Society*, **57(5A)**: p. 998-1006.
 15. Reddi Mohan Naidu, K., et al., (2012). Design, synthesis and antiviral potential of 14-aryl/heteroaryl-14H-dibenzo [a, j] xanthenes using an efficient polymer-supported catalyst. *Molecules*, **17(6)**: p. 7543-7555.
 16. Napoleon, A.A. and F.-R.N. Khan, (.2014) Potential anti-tubercular and in vitro anti-inflammatory agents: 9-substituted 1, 8-dioxo-octahydroxanthenes through cascade/domino reaction by citric fruit juices. *Medicinal Chemistry Research*, **23(11)**: p. 4749-4760.
 17. Cao, Y., et al., (2013). Solvent-free synthesis of 14-aryl-14H-dibenzo [a, j] xanthenes catalyzed by recyclable and reusable iron (III) triflate. *Research on Chemical Intermediates*, **39(7)**: p. 3055-3062.
 18. Ormond, A.B. and H.S. Freeman, (2013). Dye sensitizers for photodynamic therapy. *Materials*, **6(3)**: p. 817-840.
 19. Yoon, I., J.Z. Li, and Y.K. Shim, (2013). Advance in photosensitizers and light delivery for photodynamic therapy. *Clinical endoscopy*, **46(1)**: p. 7.
 20. Zhang, H.Q. and W.B. Euler, (2016). Detection of gas-phase explosive analytes using fluorescent spectroscopy of thin films of xanthene dyes. *Sensors and Actuators B: Chemical*, **225**: p. 553-562.
 21. Harichandran, G., S.D. Amalraj, and P. Shanmugam, (2014). Synthesis and characterization of phosphate anchored MnO₂ catalyzed solvent free synthesis of xanthene laser dyes. *Journal of Molecular Catalysis A: Chemical*, **392**: p. 31-38.
 22. Anstoetz, M., M. Clark, and L. Yee, (2016). Resolving topography of an electron beam-sensitive oxalate-phosphate-amine metal-organic framework (OPA-MOF). *Journal of materials science*, **51(3)**: p. 1562-1571.
 23. Kozhevnikov, I., et al., (1994) New acid catalyst comprising heteropoly acid on a mesoporous molecular sieve MCM-41. *Catalysis Letters*, **30(1-4)**: p. 241-252.
 24. Jauncey, G., (1924). The scattering of x-rays and Bragg's law. *Proceedings of the National Academy of Sciences of the United States of America*, **10(2)**: p. 57.
 25. Klug, H.P. and L.E. Alexander, (1974): X-ray diffraction procedures: for polycrystalline and amorphous materials. *X-Ray Diffraction Procedures: For Polycrystalline and Amorphous Materials*, 2nd Edition, by Harold P. Klug, Leroy E. Alexander, pp. 992. ISBN 0-471-49369-4. Wiley-VCH, May 1974., (p. 992.
 26. Wang, Y., et al., (1767) Preparation and characterization of perovskite LaFeO₃ nanocrystals. *Materials Letters*, 2006. **60(13-14)**: p. -1770.
 27. Wang, S., et al., (2000). Effect of heat treatment on the structure and properties of poly (2, 6-benzothiazole)(ABPBT) and poly (2, 5-benzoxazole)(ABPBO). *Journal of materials science*, **35(23)**: p. 5873-5877.
 28. Shakibaei, G.I., P. Mirzaei, and A. Bazgir, (2007). Dowex-50W promoted synthesis of 14-aryl-14H-dibenzo [a, j] xanthene and 1, 8-dioxo-octahydroxanthene derivatives under solvent-free conditions. *Applied Catalysis A: General*, **325(1)**: p. 188-192.
 29. Khaligh, N.G. and F. Shirini, (2015). N-Sulfonic acid poly (4-vinylpyridinium) hydrogen sulfate as an efficient and reusable solid acid catalyst for one-pot synthesis of xanthene derivatives in dry media under ultrasound irradiation.

- Ultrasonics sonochemistry, **22**: p. 397-403.
30. Wang, Y., et al., (2018). A Novel Tb@Sr-MOF as Self-Calibrating Luminescent Sensor for Nutritional Antioxidant. *Nanomaterials*, **8(10)**: p. 796.
 31. Manoj, B. and A. Kunjomana, (2012). Study of stacking structure of amorphous carbon by X-ray diffraction technique. *Int. J. Electrochem. Sci*, **7(4)**: p. 3127-3134.
 32. Saenger, K., et al. (2010)., In situ x-ray diffraction study of graphitic carbon formed during heating and cooling of amorphous-C/Ni bilayers. *Applied Physics Letters*, **96(15)**: p. 153105.
 33. Shekhah, O., et al., (2012) Successful implementation of the stepwise layer-by-layer growth of MOF thin films on confined surfaces: mesoporous silica foam as a first case study. *Chemical Communications*,. **48(93)**: p. 11434-11436.
 34. Sarkar, S., et al., (2015) Amino acid functionalized blue and phosphorous-doped green fluorescent carbon dots as bioimaging probe. *RSC Advances*,. **5(81)**: p. 65913-65921.
 35. Hadži, D. and N. Sheppard, (1953).The infra-red absorption bands associated with the COOH and COOD groups in dimeric carboxylic acids. I. The region from 1500 to 500 cm⁻¹. *Proceedings of the Royal Society of London. Series A. Mathematical and Physical Sciences*, **216(1125)**: p. 247-266.
 36. Reddy, S.B., et al., (2018).Fourier Transform Infrared (FTIR) Spectroscopy of Soil Humic and Fulvic Acids Extracted from Paddy Land Use System. *Int. J. Curr. Microbiol. App. Sci*, **7(5)**: p. 834-837.
 37. Wu, Y., et al., (2018.) Synthesis of rod-like metal-organic framework (MOF-5) nanomaterial for efficient removal of U (VI): batch experiments and spectroscopy study. *Science bulletin*, **63(13)**: p. 831-839.
 38. Thomas, L. and R.A. Chittenden, (1964). Characteristic infrared absorption frequencies of organophosphorus compounds—II. P—O(X) bonds. *Spectrochimica Acta*, **20(3)** : p. 489-502.
 39. Gungor, A.A., H. Nadaroglu, and D.D. Gultekin, (2019) Synthesis and Characterization of Nano-Strontium Oxide (SrO) Using Erzincan Cimin Grape (*Vitis vinifera*, Cimin). *Chemical Science International Journal*,: p. 1-7.
 40. Garrone, E., et al., (1999). Thermodynamics of CO adsorption on the zeolite Na-ZSM-5 A combined microcalorimetric and FTIR spectroscopic study. *Physical Chemistry Chemical Physics*, **1(4)**: p. 513-518.
 41. Solymosi, F. and T. Bansagi, (1995).Infrared spectroscopic study of the isocyanate surface complex over Cu-ZSM-5 catalysts. *Journal of Catalysis*, **156(1)**: p. 75-84.